Discontinuities in Planar Chirowaveguides

Xinzhang Wu, *Student Member, IEEE,* and Dwight L. Jaggard, *Fellow, IEEE*

***Abstract*—In this paper, we propose, develop, and implement an exact method to analyze the effect of discontinuities in open planar chirowaveguides. The method combines the building-block approach of multimode network theory with a rigorous mode-matching procedure. Both the scattering of discrete spectra surface-wave modes and the continuous spectra radiation and evanescent modes are discussed in this paper. The introduction of equivalent transmission-line networks brings new physical insight into the overall behavior of the discontinuities. Features such as symmetrical properties of the structure are also investigated. Based on the analysis, numerical results are displayed to demonstrate the usefulness of this approach and to discuss mode conversion and radiation characteristics of discontinuities.**

***Index Terms*—Chiral material, chriowaveguide, discontinuity, mode-matching method.**

I. Introduction

DURING the past decade, attention has been focused on electromagnetic chirality [1]–[3], and its potential application to microwave, millimeter-wave, and optical-wave guided structures. The concept of chirowaveguide was introduced in [4], [5], and the characteristics of a uniform planar chirowaveguide have been extensively investigated [6]–[10]. As a further step toward the design of versatile devices and circuits, the analysis of various discontinuities in chirowaveguides becomes significant. Mariotte and Engheta analyzed the reflection and transmission of guided electromagnetic waves at an air–chiral interface and at a chiral slab in a parallel-plate waveguide. They provided a means to measure the chirality admittance in closed waveguides [11]. Here, the open waveguide case is considered and periodic structures with large variations are examined. This provides an extension to the small perturbation case examined earlier [12]–[14].

Since the planar chirowaveguide is an open structure, in addition to the surface-wave modes, the nonsurface-wave modes comprise a continuous spectrum. In this analysis, the customary procedure of discretizing the continuous spectrum [15], [16] is followed by placing perfectly conducting walls far above and below the planar chirowaveguide, thus replacing the open region with a chiral media partially filled parallel-plate waveguide, which supports, in addition to the surface waves, an infinite number of higher nonsurface-wave modes—some propagating, and the remainder, nonpropagating. This procedure is similar to the box normalization often used in quantum mechanics. The backward (or forward) radiation power of the open discontinuity structure can be obtained by the summation of the powers of the reflected (or transmitted) higher propagating nonsurface-wave modes. Note that the presence of these bounding planes does not affect the essential physics of the scattering process.

In this paper, the scattering characteristics of the discontinuities in open planar chirowaveguides are investigated by a method which combines the building-block approach of multimode network theory with a rigorous mode-matching procedure. Introducing equivalent transmission lines both in the transverse section and in the longitudinal direction not only simplifies the mathematical manipulations but also brings new physical insight into the overall behavior of the wave-propagation phenomena. In the analysis of the eigenvalue problem of the homogeneous planar chirowaveguide, a transverse equivalent transmission-line network is introduced [10], which indicates that the right circularly polarized (RCP) wave and the left circularly polarized (LCP) wave can propagate independently in the uniform regions and couple only at the interface. Although the eigenvalue problem can be treated by the vector transmission line network [6], the physical picture of the network used here provides additional clarity. In the longitudinal analysis, the electromagnetic-field problem is transferred into the building-block multimode network problem, from which the discontinuity structure is viewed as consisting of uniform waveguides, or building blocks, and junctions. The fields are represented by the complete set of waveguide modes corresponding to independent multimode transmission lines for each uniform waveguide and are then required to satisfy the boundary conditions at each junction. Mode matching is then employed so that the coupling of the transmission lines between the two sides of the junction can be calculated. Finally, all parts of the problem are put together to obtain the scattering properties of the entire structure. In this analysis, the symmetrical properties of the discontinuity structure, both in the cross section and in the longitudinal direction, are discussed in detail so that the analysis can be simplified.

After explaining the concept and developing a mathematical formulation, numerical results of reflection, transmission, and radiation effects are carefully investigated. The coupling effect between the R_0 mode (i.e., the TE_0 mode for nonchirowaveguide) and the L_0 mode (i.e., the TM_0 mode for nonchirowaveguide) were especially considered. All the results are explained using simple underlying physical principles and may be applied to problems of practical circuit design.

Manuscript received July 8, 1996; revised January 24, 1997.

The authors are with the Complex Media Laboratory, Moore School of Electrical Engineering, University of Pennsylvania, Philadelphia, PA 19104-6390 USA.

Publisher Item Identifier S 0018-9480(97)02902-5.

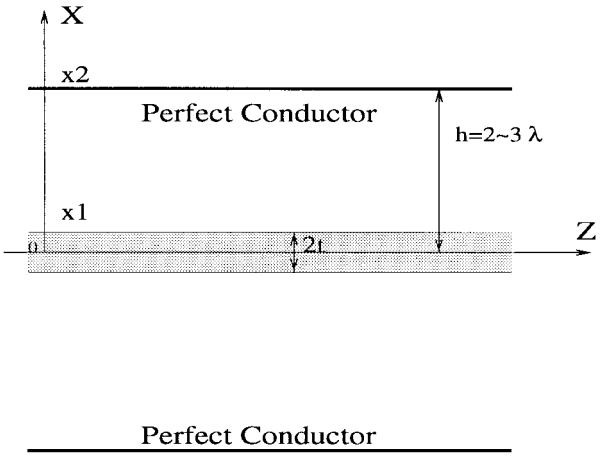

Fig. 1. Configuration of a uniform planar chirowaveguide. Here, in order to discretize the continuous spectrum, perfect conducting walls are introduced far above and below the chiral slab.

II. Equivalent Transmission-Line Representation of Homogeneous Planar Chirowaveguide

A homogeneous planar chirowaveguide of the type shown in Fig. 1 is considered. In order to analyze the discontinuity problem in the following section, both the surface-wave modes with discretized modal spectra and the radiation and evanescent modes with continuous modal spectra are considered. For mathematical simplicity the continuous spectrum is discretized. Here, perfectly conducting walls are introduced far above and below the chiral slab, and the guided wave structure becomes a planar waveguide partially filled with chiral media.

For chiral media, the constitutive relations for time-harmonic fields ($e^{j\omega t}$) may be written as [1]–[3]

$$\mathbf{D} = \epsilon \mathbf{E} - j\xi_c \mathbf{B} \tag{1a}$$

$$\mathbf{H} = \frac{\mathbf{B}}{\mu} - j\xi_c \mathbf{E} \tag{1b}$$

where ξ_c is the chirality admittance, ϵ is the permittivity, and μ is the permeability.

Substituting the above constitutive relations into Maxwell's curl equations, we obtain

$$\nabla \times \mathbf{E} = -j\omega\, \mu \mathbf{H} + \omega\kappa\sqrt{\mu\epsilon_c}\mathbf{E} \tag{2a}$$

$$\nabla \times \mathbf{H} = j\omega\epsilon_c \mathbf{E} + \omega\kappa\sqrt{\mu\epsilon_c}\mathbf{H} \tag{2b}$$

where $\epsilon_c = \epsilon + \mu\xi_c^2$, and κ is a dimensionless and normalized quantity called the chirality parameter, defined as $\kappa = \xi_c\sqrt{\mu/\epsilon_c}$.

In this analysis, we assume that the fields are invariant along the y-direction, i.e., $\partial/\partial y = 0$. From (2), we get

$$\frac{\partial}{\partial z}\begin{pmatrix} E_x \\ H_x \end{pmatrix} = -\mathbf{K}^{-1}\frac{\partial^2}{\partial z^2}\begin{pmatrix} E_y \\ H_y \end{pmatrix} \tag{3}$$

$$\frac{\partial}{\partial z}\begin{pmatrix} E_y \\ H_y \end{pmatrix} = -\mathbf{K}\begin{pmatrix} E_x \\ H_x \end{pmatrix} \tag{4}$$

$$\frac{\partial}{\partial x}\begin{pmatrix} E_z \\ H_z \end{pmatrix} = -\mathbf{K}\begin{pmatrix} E_y \\ H_y \end{pmatrix} - \mathbf{K}^{-1}\frac{\partial^2}{\partial z^2}\begin{pmatrix} E_y \\ H_y \end{pmatrix} \tag{5}$$

$$\frac{\partial}{\partial x}\begin{pmatrix} E_y \\ H_y \end{pmatrix} = \mathbf{K}\begin{pmatrix} E_z \\ H_z \end{pmatrix} \tag{6}$$

where

$$\mathbf{K} = \begin{bmatrix} \omega\kappa\sqrt{\mu\epsilon_c} & -j\omega\,\mu \\ j\omega\epsilon_c & \omega\kappa\sqrt{\mu\epsilon_c} \end{bmatrix} \tag{7a}$$

and

$$\mathbf{K}^{-1} = \frac{1}{\omega^2\,\mu\epsilon_c(\kappa^2-1)}\begin{bmatrix} \omega\kappa\sqrt{\mu\epsilon_c} & j\omega\,\mu \\ -j\omega\epsilon_c & \omega\kappa\sqrt{\mu\epsilon_c} \end{bmatrix}. \tag{7b}$$

To separate variables, let

$$E_x = e_x(x)U(z) \tag{8a}$$

$$H_x = h_x(x)U(z) \tag{8b}$$

$$E_y = e_y(x)J(z) \tag{8c}$$

$$H_y = h_y(x)J(z) \tag{8d}$$

$$E_z = e_z(x)J(z) \tag{8e}$$

$$H_z = h_z(x)U(z) \tag{8f}$$

and substitute into (3)–(6). We find

$$\begin{cases} \dfrac{dU(z)}{dz} = -jk_z Z_c J(z) \\ \dfrac{dJ(z)}{dz} = -jk_z Y_c U(z) \end{cases} \tag{9}$$

and

$$\begin{pmatrix} e_x \\ h_x \end{pmatrix} = jk_z\mathbf{K}^{-1}\begin{pmatrix} e_y \\ h_y \end{pmatrix} \tag{10}$$

$$\frac{d}{dx}\begin{pmatrix} e_z \\ h_z \end{pmatrix} = -\mathbf{K}\begin{pmatrix} e_y \\ h_y \end{pmatrix} + k_z^2\mathbf{K}^{-1}\begin{pmatrix} e_y \\ h_y \end{pmatrix} \tag{11}$$

$$\frac{d}{dx}\begin{pmatrix} e_y \\ h_y \end{pmatrix} = \mathbf{K}\begin{pmatrix} e_z \\ h_z \end{pmatrix} \tag{12}$$

where Z_c is the characteristic impedance which is normalized as

$$Z_c = \frac{1}{Y_c} = 1.0 \tag{13}$$

in this model. Equation (9) is the equivalent transmission line equation in the z-direction. Here, $U(z)$ and $J(z)$ are the voltage and current amplitudes of the eigenmode in the planar chirowaveguide, and k_z is the longitudinal propagation constant of the eigenmode.

The matrix $\mathbf{K}$ and its inverse matrix $\mathbf{K}^{-1}$ in (10) and (11) can be transformed into a diagonal matrix by means of a transformation matrix $\mathbf{T}$ as follows:

$$\mathbf{T}^{-1}\mathbf{K}\mathbf{T} = \begin{bmatrix} k_+ & 0 \\ 0 & -k_- \end{bmatrix} \tag{14a}$$

and

$$\mathbf{T}^{-1}\mathbf{K}^{-1}\mathbf{T} = \begin{bmatrix} \dfrac{1}{k_+} & 0 \\ 0 & \dfrac{-1}{k_-} \end{bmatrix} \tag{14b}$$

where

$$k_\pm = \omega\sqrt{\mu\epsilon_c}(1 \pm \kappa) \tag{15}$$

$$\mathbf{T} = \begin{bmatrix} 1 & 1 \\ j\sqrt{\dfrac{\epsilon_c}{\mu}} & -j\sqrt{\dfrac{\epsilon_c}{\mu}} \end{bmatrix}, \qquad \mathbf{T}^{-1} = \frac{1}{2}\begin{bmatrix} 1 & -j\sqrt{\dfrac{\mu}{\epsilon_c}} \\ 1 & j\sqrt{\dfrac{\mu}{\epsilon_c}} \end{bmatrix}. \tag{16}$$

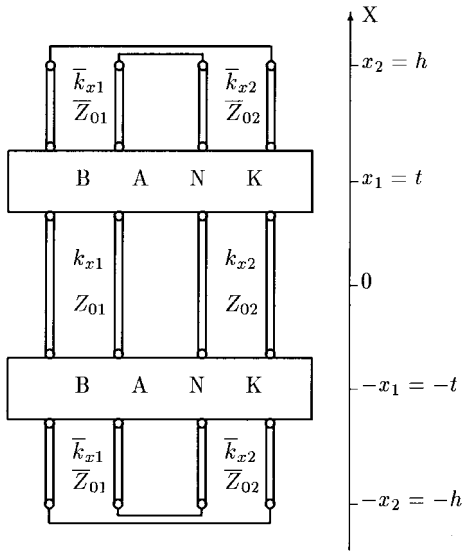

Fig. 2. Transmission-line network representation of Fig. 1.

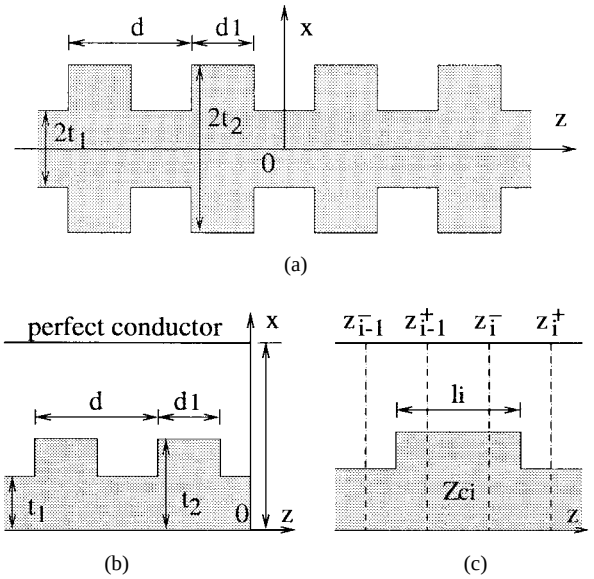

Fig. 3. (a) Configuration of a chirowaveguide grating. (b) Bisection due to symmetry. (c) ith basic unit of (b).

If we let

$$\begin{bmatrix} e_y(x) \\ h_y(x) \end{bmatrix} = \mathbf{T} \begin{bmatrix} V_1(x) \\ V_2(x) \end{bmatrix} \tag{17a}$$

and

$$\begin{bmatrix} e_z(x) \\ h_z(x) \end{bmatrix} = \mathbf{T} \begin{bmatrix} I_1(x) \\ I_2(x) \end{bmatrix} \tag{17b}$$

the uncoupled radial transmission lines for the RCP wave ($i = 1$) and LCP wave ($i = 2$) can be obtained as

$$\begin{cases} \dfrac{dV_i(x)}{dx} = -jk_{xi}Z_{0i}I_i(x) \\ \dfrac{dI_i(x)}{dx} = -jk_{xi}Y_{0i}V_i(x) \end{cases} \tag{18}$$

where

$$Z_{01} = \frac{1}{Y_{01}} = \frac{jk_+}{k_{x1}}, \qquad k_{x1}^2 = k_+^2 - k_z^2 \tag{19}$$

$$Z_{02} = \frac{1}{Y_{02}} = \frac{-jk_-}{k_{x2}}, \qquad k_{x2}^2 = k_-^2 - k_z^2. \tag{20}$$

The equivalent transmission-line network in the cross section is depicted in Fig. 2. In that figure, the RCP wave and the LCP wave can propagate independently in the uniform regions and couple only at the interface [10]. The introduction of the transmission line brings a clear physical picture of wave propagation in the planar chirowaveguides. Since the structure under consideration is symmetrical to the $x = 0$ plane, the eigenmodes of planar chirowaveguide can be divided into two types. The first type, which is defined as the even modes (i.e., R_{2m} modes and L_{2m} modes), corresponds to the open-circuit in the transmission line at $x = 0$, while the second type defined as the odd modes (i.e., R_{2m-1} modes and L_{2m-1} modes) corresponds to the short-circuit in the transmission line at $x = 0$. The nomenclature of R_n modes and L_n modes was chosen because it can be shown that when chirality is present, R_n modes carry most of its energy in the RCP guided-wave component and L_n modes carry most of its energy in the LCP guided-wave component [9]. Here, it should be noted that the short-circuit (open-circuit) does not indicate that the plane at $x = 0$ is a physical electric wall (magnetic wall) or $E_y = 0$ and $E_z = 0$ ($H_y = 0$ and $H_z = 0$), but indicates the equivalent transmission line is short-circuit (open-circuit) or $E_y = 0$ and $H_y = 0$ ($E_z = 0$ and $H_z = 0$). The purpose of dividing the modes into the even type and odd type is that if the discontinuity structure to be studied is symmetrical to the $x = 0$ plane, for the even-modes' (odd-modes') excitation case only the even modes (odd modes) can be generated so that only one type of modes is considered; thus simplifying the analysis procedure. The eigenvalues and eigenfunctions of a planar chiral waveguide can be obtained using the transverse resonance method and transmission-line theory, which is not discussed here because of space limitation.

III. Scattering Characteristics of Discontinuities in the Longitudinal Direction

As an example of the discontinuities in planar chirowaveguides, Fig. 3(a) shows a geometrical configuration of the chirowaveguide grating under consideration. Because the structure is symmetrical in the longitudinal direction, the scattering of the guided mode may be analyzed in terms of the symmetrical and antisymmetrical excitations for which we have the equivalent transmission-line open-circuit and short-circuit bisections in the longitudinal transmission lines, respectively, as indicated in Fig. 3(b). It should also be noted that the short-circuit (open-circuit) does not indicate that the plane at $z = 0$ is a physical electric wall (magnetic wall) or $E_x = 0$ and $E_y = 0$ ($H_x = 0$ and $H_y = 0$), but indicates the equivalent transmission line is short-circuit (open-circuit) or $E_x = 0$ and $H_x = 0$ ($E_y = 0$ and $H_y = 0$). Here, we consider only the even-mode excitation case so that the plane of $x = 0$ corresponds to equivalent transmission-line open-circuit.

The scattering properties of each bisection can be investigated through the reflection characteristics of each basic unit. Fig. 3(c) depicts the ith basic unit which consists of the ith step

discontinuity between two uniform guides at a point $z = z_i$ and a uniform guide of length l_i between points z_i and z_{i-1}. The analysis procedure for the reflection characteristics of the basic unit is outlined below.

Since the terminal plane of the stepped structure at $z = 0$ for the longitudinal equivalent transmission lines is either open-circuit or short-circuit in the equivalent transmission line, the input impedance matrix $\mathbf{Z}(z_i^+)$ at the $z = z_i^+$ plane looking to the right can be determined by the impedance transform technique. Therefore, $\mathbf{Z}(z_i^+)$ can be considered as a known matrix. General field solution in each constituent uniform region may be expressed in terms of the superposition of a complete set of mode functions. For tangential field components in the $z < z_i^-$ region, we have

$$\begin{bmatrix} E_x(x, z) \\ H_x(x, z) \end{bmatrix} = \sum_{n=1}^{\infty} \begin{bmatrix} e_{xn}(x) \\ h_{xn}(x) \end{bmatrix} U_n(z) \tag{21}$$

$$\begin{bmatrix} E_y(x, z) \\ H_y(x, z) \end{bmatrix} = \sum_{n=1}^{\infty} \begin{bmatrix} e_{yn}(x) \\ h_{yn}(x) \end{bmatrix} J_n(z). \tag{22}$$

A similar set of tangential field components may also be written for the $z > z_i^+$ region, but it is not cited here for simplicity. It can be demonstrated that the orthogonal relation between two normalized modes in the homogeneous planar chirowaveguide are expressed as [17]

$$\int_0^h (e_{xm}h_{yn} + e_{yn}h_{xm})\, dx = \delta_{mn} \tag{23}$$

where δ_{ij} is the Kroneker's delta function.

At the step discontinuity $z = z_i$, the tangential field components must be continuous. From (21) and (22), we obtain

$$\sum_{n=1}^{\infty} \begin{bmatrix} e_{xn}(x) \\ h_{xn}(x) \end{bmatrix} U_n(z_i) = \sum_{n=1}^{\infty} \begin{bmatrix} \overline{e}_{xn}(x) \\ \overline{h}_{xn}(x) \end{bmatrix} \overline{U}_n(z_i) \tag{24}$$

$$\sum_{n=1}^{\infty} \begin{bmatrix} e_{yn}(x) \\ h_{yn}(x) \end{bmatrix} J_n(z_i) = \sum_{n=1}^{\infty} \begin{bmatrix} \overline{e}_{yn}(x) \\ \overline{h}_{yn}(x) \end{bmatrix} \overline{J}_n(z_i). \tag{25}$$

The quantities with overbars indicate those on the right-hand side (RHS) of the discontinuity. Above four equations hold for any x at $z = z_i$ within the enclosure. Multiplying (24) and (25) by $[h_{ym}, e_{ym}]$ and $[h_{xm}, e_{xm}]$, respectively, and making use of the orthogonality relation (23), we obtain

$$\mathbf{U} = \mathbf{M}_i \overline{\mathbf{U}}, \qquad \mathbf{J} = \mathbf{N}_i \overline{\mathbf{J}} \tag{26}$$

where $\mathbf{U}$ and $\mathbf{J}$ are column vectors whose elements are transmission-line voltage and current of the nth mode, $U_n(z_i)$ and $J_n(z_i)$; similar definitions hold for those vectors with an overbar. The $\mathbf{M}_i$ and $\mathbf{N}_i$ are matrices characterizing the coupling of modes at the step discontinuity, and their elements are defined by scalar products or overlap integrals of mode functions on the two sides of the discontinuity as follows:

$$(\mathbf{M}_i)_{mn} = \int_0^h (e_{ym}\overline{h}_{xn} + \overline{e}_{xn}h_{ym})\, dx$$

$$(\mathbf{N}_i)_{mn} = \int_0^h (\overline{e}_{yn}h_{xm} + e_{xm}\overline{h}_{yn})\, dx$$

for $m, n = 1, 2, 3, \cdots$. On the other hand, multiplying (24) and (25) by $[\overline{h}_{ym}, \overline{e}_{ym}]$ and $[\overline{h}_{xm}, \overline{e}_{xm}]$, respectively, and making use of the orthogonality relation (23) of the chirowaveguide on the RHS of the discontinuity, we find

$$\mathbf{N}_i^T \mathbf{U} = \overline{\mathbf{U}}, \qquad \mathbf{M}_i^T \mathbf{J} = \overline{\mathbf{J}}. \tag{27}$$

One can show that the following matrix identities hold for the present case:

$$\mathbf{M}_i^T \mathbf{N}_i = \mathbf{N}_i^T \mathbf{M}_i = \mathbf{1} \tag{28}$$

where $\mathbf{1}$ is the unit matrix and T denotes the transpose.

From (26) and (27), it can be derived that the input impedance matrix $\mathbf{Z}(z_i^-)$ at the $z = z_i^-$ plane looking to the right satisfies

$$\mathbf{Z}(z_i^-) = \mathbf{M}_i \mathbf{Z}(z_i^+) \mathbf{M}_i^T \tag{29}$$

where

$$\mathbf{U} = \mathbf{Z}(z_i^-)\mathbf{J}, \qquad \overline{\mathbf{U}} = \mathbf{Z}(z_i^+)\overline{\mathbf{J}}. \tag{30}$$

The reflection-coefficient matrix $\mathbf{\Gamma}(z_i^-)$ at the $z = z_i^-$ plane looking to the right is obtained as

$$\mathbf{\Gamma}(z_i^-) = [\mathbf{Z}(z_i^-) + \mathbf{Z}_{ci}]^{-1}[\mathbf{Z}(z_i^-) - \mathbf{Z}_{ci}] \tag{31}$$

and the input-impedance matrix at the $z = z_{i-1}^+$ plane looking to the right is determined by the impedance-transform technique as [16]

$$\mathbf{Z}(z_{i-1}^+) = \mathbf{Z}_{ci}[\mathbf{1} + \mathbf{H}_i \mathbf{\Gamma}_i \mathbf{H}_i][\mathbf{1} - \mathbf{H}_i \mathbf{\Gamma}_i \mathbf{H}_i]^{-1}. \tag{32}$$

Here, $\mathbf{Z}_{ci}$ and $\mathbf{H}_i$ are the characteristic impedance and phase matrices of the ith step discontinuity and they are all diagonal matrices with elements

$$(Z_{ci})_{mn} = \delta_{mn} Z_{cin} \tag{33a}$$

$$(H_i)_{mn} = \delta_{mn} \exp(-jk_{zin}l_i) \tag{33b}$$

where k_{zin} and Z_{cin} are the wavenumber in the z-direction and the characteristic impedance for the nth mode in the ith chirowaveguide section, respectively.

With the bisections in the z-direction, there are two different combinations of boundary conditions. For an incident guided mode from the input waveguide, we analyze the two separate substructures with the respective boundary conditions. In each case, the energy is totally reflected and the reflection-coefficient matrix are denoted by $\mathbf{R_o}$ and $\mathbf{R_s}$ for the equivalent transmission line open-circuit and short-circuit bisections, respectively. After determining $\mathbf{R_o}$ and $\mathbf{R_s}$ by using (29)–(32), the scattering-coefficient matrices of the entire structure are determined by

$$\mathbf{R} = \frac{\mathbf{R_o} + \mathbf{R_s}}{2}, \qquad \mathbf{T} = \frac{\mathbf{R_o} - \mathbf{R_s}}{2} \tag{34}$$

where $\mathbf{R}$ is the reflection-coefficient matrix of the input waveguide and $\mathbf{T}$ is the transmission-coefficient matrix from the input to the output waveguide.

If the incident wave is assumed to be the nth surface-wave mode of the input waveguide with power 1.0, then the reflected power P_{rm} of the mth mode in the input waveguide and the

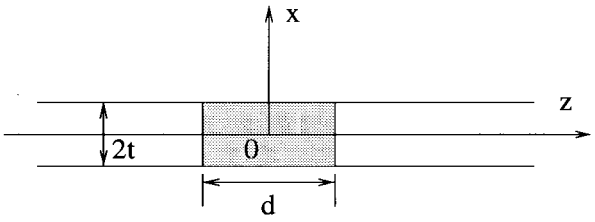

Fig. 4. Configuration of a uniform planar chirowaveguide sandwiched between two identical nonchirowaveguides.

transmitted power P_{tk} of the kth mode in the output waveguide can be determined, respectively, by

$$P_{rm} = \frac{|R_{mn}|^2 \operatorname{Re}\left[\int_0^h (e_{xm}h_{ym}^* - e_{ym}h_{xm}^*)\,dx\right]}{\operatorname{Re}\left[\int_0^h (e_{xn}h_{yn}^* - e_{yn}h_{xn}^*)\,dx\right]} \quad (35)$$

$$P_{tk} = \frac{|T_{kn}|^2 \operatorname{Re}\left[\int_0^h (e_{xk}h_{yk}^* - e_{yk}h_{xk}^*)\,dx\right]}{\operatorname{Re}\left[\int_0^h (e_{xn}h_{yn}^* - e_{yn}h_{xn}^*)\,dx\right]}. \quad (36)$$

IV. Examples and Discussion

A. Mode Conversion by Planar Chirowaveguide Sandwiched Between Two Non-Chirowaveguides

To observe the mode-conversion properties due to electromagnetic chirality, we examine a uniform planar chirowaveguide sandwiched between two identical nonchirowaveguides as depicted in Fig. 4. The chirowaveguide has the same dielectric constant, permeability, and thickness as those of the nonchirowaveguides, but the chirality is nonzero. If the chirality vanishes, the whole structure is a uniform nonchirowaveguide and no mode conversion, reflection, and radiation phenomena will occur. If the chirality does not vanish, the reflection and transmission wave will contain both TE_0 mode and TM_0 mode even if the incident mode is a single TE_0 mode or TM_0 mode, and radiation will also occur. In the following, the effect of chirality and the normalized width of the chirowaveguide d/λ is carefully discussed by fixing $\epsilon_c = 10\epsilon_0$, $\mu = \mu_0$, and $t = 0.15\lambda$. Here, we discuss only TE_0 mode incidence case. Since chiral media is reciprocal and the structure is symmetric, the reflection and transmission of TM_0 mode when the incident mode is TE_0 mode should be the same as the reflection and transmission of TE_0 mode when the incident mode is TM_0 mode.

Fig. 5 illustrates the reflection, transmission, and radiation properties of TE_0 incidence case. Here, a small value of $\kappa = 0.02$ is chosen. At first, from Fig. 5(e) and (f), we see that the percentage of backward and forward radiation power remains very small as d/λ changes, which indicates in this calculation, two modes (TE_0 and TM_0 for nonchirowaveguide, and R_0 and L_0 for chirowaveguide) are good enough to get the solutions of Fig. 5(a)–(d) while in this calculation, we take 20 modes to get precise radiation power. We may also find in this case, that the reflection powers are also very small. From Fig. 5, we finally know that when d/λ changes, the incident TE_0 mode will partially transfer to output TM_0 mode and the maximum transferred power is only 34% in this small chirality case.

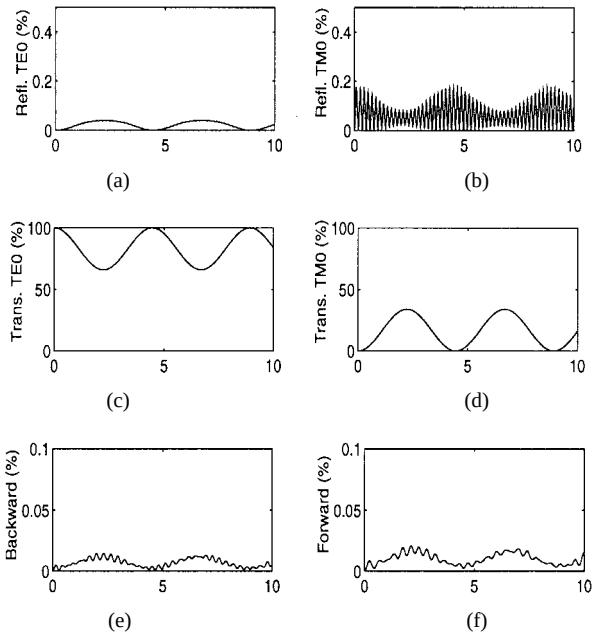

Fig. 5. When the incident mode of Fig. 4 is TE_0 mode and the chirality parameter is taken to be a small value $\kappa = 0.02$, the percentage power of (a) reflected TE_0 mode, (b) reflected TM_0 mode, (c) transmitted TE_0 mode, (d) transmitted TM_0 mode, (e) backward radiation, and (f) forward radiation versus normalized length of chirowaveguide d/λ is shown.

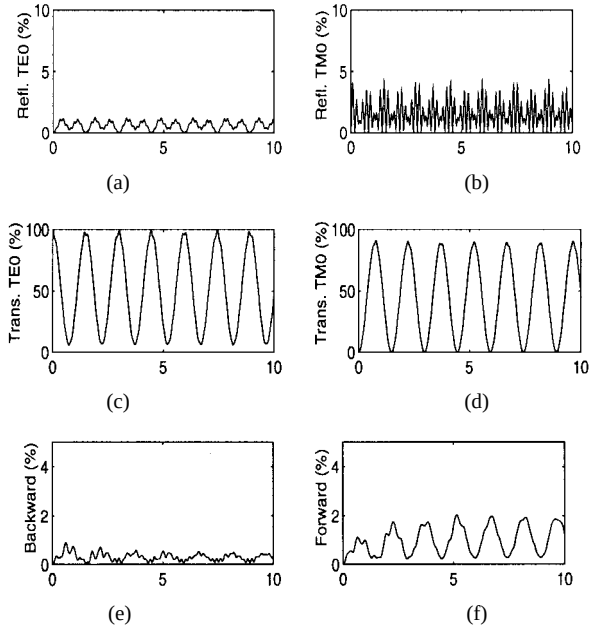

Fig. 6. When the incident mode of Fig. 4 is TE_0 mode and the chirality parameter is taken to be a medium value $\kappa = 0.1$, the percentage power of (a) reflected TE_0 mode, (b) reflected TM_0 mode, (c) transmitted TE_0 mode, (d) transmitted TM_0 mode, (e) backward radiation, and (f) forward radiation versus normalized length of chirowaveguide d/λ is shown.

Fig. 6 examines TE_0 mode incidence for a moderate value of $\kappa = 0.1$. In this case, we still find that the radiation

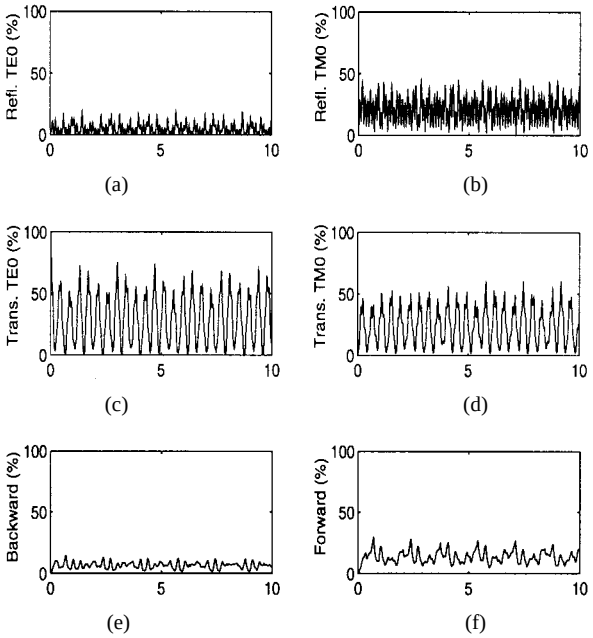

Fig. 7. When the incident mode of Fig. 4 is TE_0 mode and the chirality parameter is taken to be a large value $\kappa = 0.4$, the percentage power of (a) reflected TE_0 mode, (b) reflected TM_0 mode, (c) transmitted TE_0 mode, (d) transmitted TM_0 mode, (e) backward radiation, and (f) forward radiation versus normalized length of chirowaveguide d/λ is shown.

and reflection are not very strong, but the mode conversion becomes faster, and the maximum converted power can be as large as 91%. In Fig. 7, a large value of $\kappa = 0.4$, is chosen, finding that the mode conversion becomes much faster, but the maximum converted power can only be 67% because of strong radiation and reflection. From these figures, we can draw the conclusion that if we want to use chirowaveguide as mode-conversion devices, the chirality should be chosen to be a moderate value as indicated in Fig. 6.

B. Guided Wave Propagation Through Double-Step Discontinuity and Air Gap

Now, guided wave propagation through double-step discontinuity depicted in Fig. 8(a) is discussed. If no step exists, the structure is a uniform chirowaveguide and no mode conversion, reflection, and radiation will occur. Also, as in the normal incidence case discussed here, if the chirality vanishes, the waveguides become nonchirowaveguides or ordinary dielectric waveguides, and no mode conversion effect will occur. This means that if the incident mode is TE_0 mode (or TM_0 mode), the reflection, transmission and radiation mode can only be TE polarized (or TM polarized). Fig. 9 shows the reflection, transmission, and radiation properties of R_0 mode incidence case. Here, we choose $\epsilon_c = 2.25\epsilon_0, \mu = \mu_0, \kappa = 0.1, t_1 = 0.15\lambda$, and $t_2 = 0.30\lambda$. From the figures, we see both the effects of mode conversion and radiation.

Propagation properties of the air gap shown in Fig. 8(b) are discussed in Figs. 10 and 11 for R_0 mode and L_0 mode incidence, respectively. Here, we choose $\epsilon_c = 5\epsilon_0, \mu = \mu_0, \kappa = 0.4$, and $t = 0.15\lambda$. As we can expect, when the distance of the two waveguides increases, they become unrelated and, therefore, the transmission power of incident

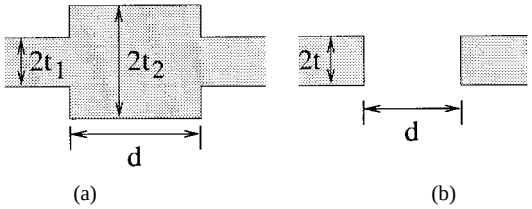

Fig. 8. Configuration of (a) planar chirowaveguide double-step discontinuity and (b) two planar chirowaveguides separated by an air gap.

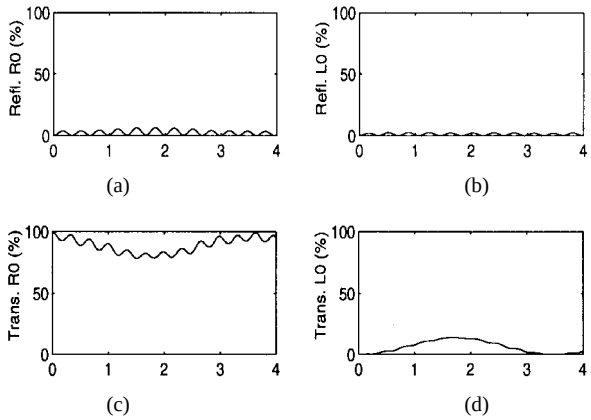

Fig. 9. When the incident mode of Fig. 8(a) is R_0 mode, the percentage power of (a) reflected R_0 mode, (b) reflected L_0 mode, (c) transmitted R_0 mode, (d) transmitted L_0 mode, (e) backward radiation, and (f) forward radiation versus normalized length of d/λ is shown.

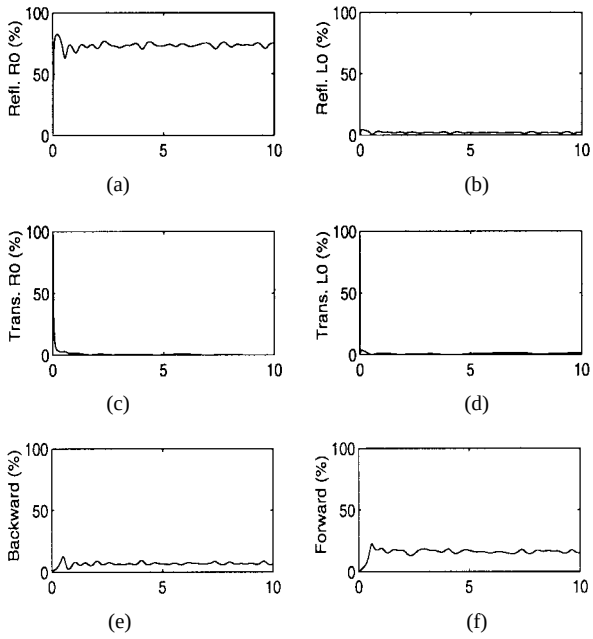

Fig. 10. When the incident mode of Fig. 8(b) is R_0 mode, the percentage power of (a) reflected R_0 mode, (b) reflected L_0 mode, (c) transmitted R_0 mode, (d) transmitted L_0 mode, (e) backward radiation, and (f) forward radiation versus normalized length of d/λ is shown.

mode goes down as shown in Figs. 10(c) and 11(d). Here the transmission power of converted mode shown in Figs. 10(d) and 11(c) always keep a small value. There is a difference between Figs. 10 and 11. In Fig. 10, since the incident mode R_0 has an effective dielectric constant $\epsilon_{eR} = (k_{zR}/k_0)^2 =$

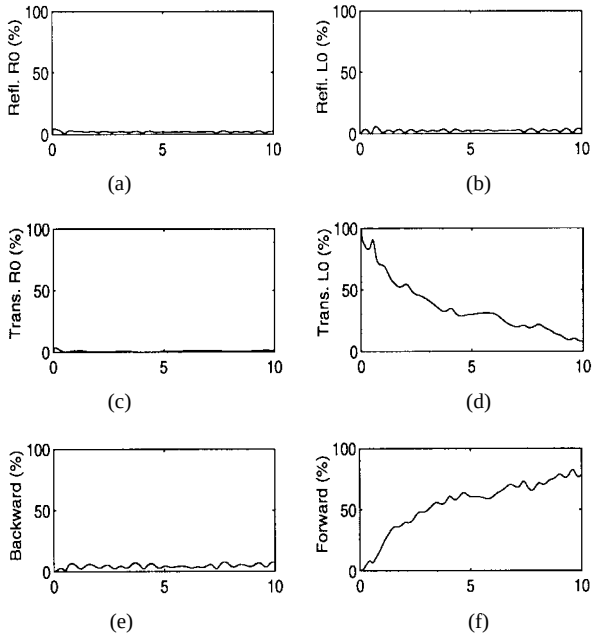

Fig. 11. When the incident mode of Fig. 8(b) is L_0 mode, the percentage power of (a) reflected R_0 mode, (b) reflected L_0 mode, (c) transmitted R_0 mode, (d) transmitted L_0 mode, (e) backward radiation, and (f) forward radiation versus normalized length of d/λ is shown.

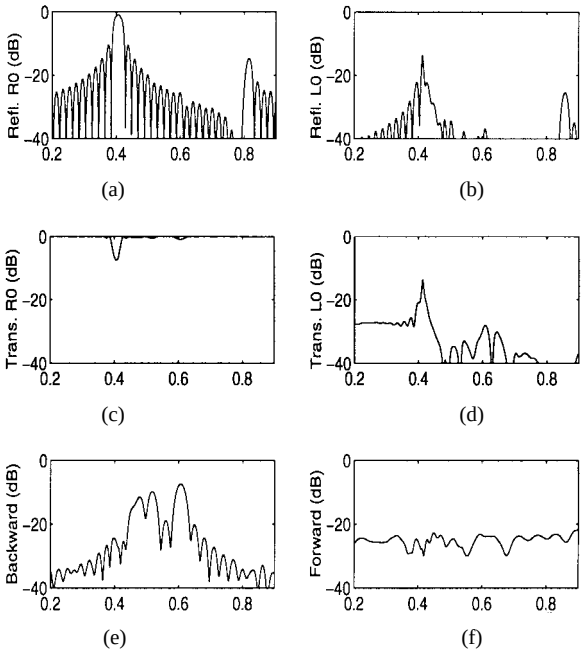

Fig. 12. When the incident mode of the periodic structure given in Fig. 3(a) is R_0 mode, the normalized power (in dB) of (a) reflected R_0 mode, (b) reflected L_0 mode, (c) transmitted R_0 mode, (d) transmitted L_0 mode, (e) backward radiation, and (f) forward radiation versus normalized period of d/λ is shown.

7.6518, which is much larger than the dielectric constant 1.0 of the air, reflection of R_0 mode assumes main effect and goes up quickly as d increases and then keeps a large value, although there are small oscillations [see Fig. 10(a)]. While for Fig. 11, since the incident mode L_0 has an effective dielectric constant $\epsilon_{eL} = (k_{zL}/k_0)^2 = 1.2416$, which is near the dielectric constant 1.0 of the air, the forward radiation assumes main effect and goes up as d increases [see Fig. 11(f)].

C. Guided Wave Propagation Through Periodic Structure with Finite Length

Guided wave propagation properties, through a periodic structure with finite length as given in Fig. 3(a), are now considered. Here, we choose $\epsilon_c = 2.25\epsilon_0$, $\mu = \mu_0$, $\kappa = 0.01$, $t_1 = \lambda/3\pi$, $t_2 = \lambda/2\pi$, and $d_1 = d/2$. Figs. 12 and 13 show reflection, transmission, and radiation characteristics of the finite-length periodic structure with 20 corrugations versus normalized period d/λ.

The first Bragg reflection peak can be explained by simple physics. From the Bloch theorem, the propagation of electromagnetic waves in a periodic chirowaveguide can be viewed as a uniform waveguide in the passband with the Bloch wavenumber of the periodic structure as its propagation constant. Since both the R_0 mode and the L_0 mode exist if chirality is nonzero, we may obtain two Bloch wavenumbers; one is for R_0 mode (denoted as k_{zR}) and the other is for L_0 mode (denoted as k_{zL}). Here, k_{zR} and k_{zL} can be approximately obtained as the average of the two constitutive waveguides in one periodic cell, i.e., $k_{zR} \doteq (k_{zR1} + k_{zR2})/2$, and $k_{zL} \doteq (k_{zL1} + k_{zL2})/2$. The first Bragg reflection point of R_0–R_0 coupling should occur at $k_{zR} \cdot 2d = 2\pi$, from which we may obtain $(d/\lambda)_{R_0-R_0} \doteq 0.4056$, which agrees well with Fig. 12(a). The first Bragg reflection point of L_0–L_0 coupling

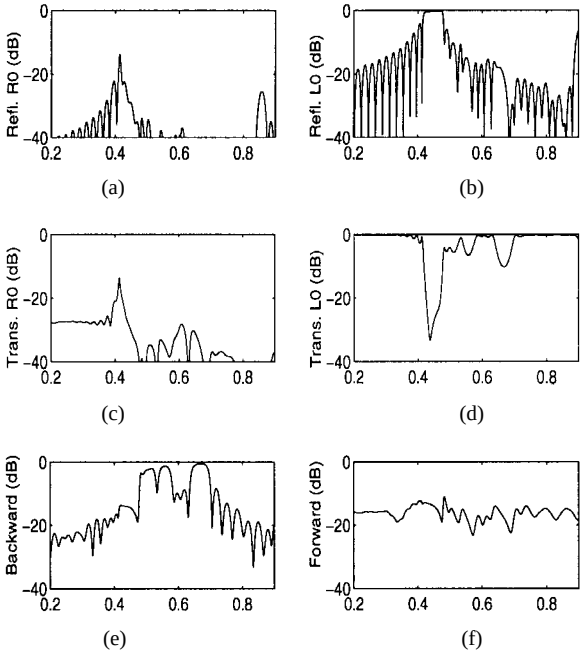

Fig. 13. When the incident mode of the periodic structure given in Fig. 3(a) is L_0 mode, the normalized power (in dB) of (a) reflected R_0 mode, (b) reflected L_0 mode, (c) transmitted R_0 mode, (d) transmitted L_0 mode, (e) backward radiation, and (f) forward radiation versus normalized period of d/λ is shown.

should occur at $k_{zL} \cdot 2d = 2\pi$, from which one may obtain $(d/\lambda)_{L_0-L_0} \doteq 0.4477$, which agrees well with Fig. 13(b). The first Bragg reflection point of R_0–L_0 and L_0–R_0 coupling should occur at $k_{zL} \cdot d + k_{zR} \cdot d = 2\pi$, from which we may obtain $(d/\lambda)_{R_0-L_0,\ L_0-R_0} \doteq 0.4256$, which agrees well with Figs. 12(b) and 13(c).

The radiation properties will now be explained. Since in the air region of Fig. 3(a) $k_{xn}^2 = k_0^2 - k_{zn}^2$ with $k_{zn} = k_z + 2n\pi/d$, when k_{xn}^2 is positive, i.e., k_{xn} is real, the nth space harmonic will radiate, from which one may obtain the backward radiation condition for the $n = -1$ space harmonic of R_0 mode and L_0 are $-k_0 < k_{zR-1} = k_{zR} - 2\pi/d < 0$ and $-k_0 < k_{zL-1} = k_{zL} - 2\pi/d < 0$, respectively, which gives $0.4479 < (d/\lambda)_R < 0.8112$ and $0.4724 < (d/\lambda)_L < 0.8954$. From Figs. 12(e) and 13(e), one may see that this physically based prediction is correct.

V. Conclusion

Equivalent networks have been introduced in both the cross section and longitudinal direction to analyze propagation properties of discontinuities in open planar chirowaveguides. Symmetry properties of the structure have also been discussed. Numerical results of mode conversion by planar chirowaveguide sandwiched between two nonchirowaveguides have shown that when the chirality parameter is small, mode conversion is weak and when the chirality parameter is moderate, mode conversion is strong; however, when the chirality parameter is large, mode conversion becomes weak again due to strong radiation and reflection. Therefore, if one wants to use chirowaveguide as a mode-conversion device, the chirality parameter should be chosen to be of moderate value.

Guided wave propagation has also been examined through double-step discontinuity and air gap. Both the mode conversion effect and radiation effect occur. Especially for the air gap, one finds a difference between R_0-mode incidence and L_0-mode incidence. When the distance of the air gap increases, the reflection of R_0 mode dominates if the incident mode is R_0 mode, while the forward radiation dominates if the incident mode is L_0 mode.

Finally, propagation properties of periodic structure with finite-length are studied and the first Bragg reflection peaks of R_0–R_0, L_0–L_0, R_0–L_0, and L_0–R_0 coupling are found. The positions of these peaks are confirmed by simple physical reasoning and support the numerical results. In addition, the limits of the radiation are evaluated and agree well with calculations.

References

[1] D. L. Jaggard, A. R. Mickelson, and C. H. Papas, "On electromagnetic waves in chiral media," *Appl. Phys.*, vol. 18, pp. 211–216, 1979.

[2] D. L. Jaggard and N. Engheta, "Chirality in electrodynamics: Modeling and applications," in *Directions in Electromagnetic Wave Modeling*, H. L. Bertoni and L. B. Felson, Eds. New York: Plenum, 1991, pp. 435–446.

[3] H. N. Kritikos, N. Engheta, and D. L. Jaggard, "Symmetry in material media," in *Symmetry in Electromagnetics*, C. Baum and H. N. Kritikos, Eds. Washington, DC: Taylor and Francis, 1995, ch 4.

[4] N. Engheta and P. Pelet, "Modes in chirowaveguides," *Opt. Lett.*, vol. 14, pp. 593–595, June 1989.

[5] P. Pelet and N. Engheta, "The theory of chirowaveguides," *IEEE Trans. Antennas Propagat.*, vol. 38, pp. 90–98, Jan. 1990.

[6] M. I. Oksanen, P. K. Koivisto, and S. A. Tretyakov, "Vector circuit method applied for chiral slab waveguide," *J. Lightwave Technol.*, vol. 10, pp. 150–155, Feb. 1992.

[7] M. I. Oksanen, P. K. Koivisto, and I. V. Lindell, "Dispersion curves and fields for a chiral slab waveguide," *Proc. Inst. Elect. Eng.*, vol. 138, pt. H, pp. 327–334, Aug. 1991.

[8] H. Cory and I. Rosenhouse, "Electromagnetic wave propagation along a chiral slab," *Proc. Inst. Elect. Eng.*, vol. 138, pt. H, pp. 51–54, Feb. 1991.

[9] K. Flood and D. L. Jaggard, "Single-mode operation in symmetric planar waveguides using isotropic chiral media," *Opt. Lett.*, vol. 21, pp. 474–476, 1996.

[10] S. Xu, K. Du, and X. Wu, "A new network method for analyzing the dispersion characteristics of multilayer planar chirowaveguide," in *Proc. Nat. Microwave Conf.*, Hefei, China, Oct. 1993, pp. 393–396, (in Chinese).

[11] F. Mariotte and N. Engheta, "Reflection and transmission of guided electromagnetic waves at an air–chiral interface and at a chiral slab in a parallel-plate waveguide," *IEEE Trans. Microwave Theory Tech.*, vol. 41, pp. 1895–1906, Nov. 1993.

[12] D. L. Jaggard, N. Engheta, M. H. Kowarz, P. Pelet, J. Liu, and Y. Kim, "Periodic chiral structures," *IEEE Trans. Antennas Propagat.*, vol. 36, pp. 1447–1452, Nov. 1989.

[13] K. Flood and D. L. Jaggard, "Distributed feedback lasers in chiral media," *IEEE J. Quantum Electron.*, vol. 30, pp. 339–345, Feb. 1994.

[14] ——, "Bandgap structure for periodic chiral media," *J. Opt. Soc. Amer. A, Opt. Image Sci.*, vol. 13, pp. 1395–1406, 1996.

[15] S. T. Peng and A. A. Oliner, "Guidance and leakage properties of a class of open dielectric waveguides: Part I—Mathematical formulations," *IEEE Trans. Microwave Theory Tech.*, vol. MTT-29, pp. 843–855, Sept. 1981.

[16] S. Xu, X. Wu, and T. Yoneyama, "Scattering of guided wave by discontinuities in NRD guide," in *Proc. Inst. Elect. Eng.*, vol. 141, pt. H, no. 3, pp. 205–210, June 1994.

[17] C. R. Paiva and A. M. Barbosa, "A linear-operator formalism for the analysis of inhomogeneous biisotropic planar waveguides," *IEEE Trans. Microwave Theory Tech.*, vol. 40, pp. 672–678, Apr. 1993.

Xinzhang Wu (S'96), photograph and biography not available at time of publication.

Dwight L. Jaggard (S'68–M'77–SM'86–F'91), photograph and biography not available at time of publication.